

Dynamical quantum phase transition and thermal equilibrium in the lattice Thirring model

Mari Carmen Bañuls,^{1,2,*} Krzysztof Cichy,^{3,†} Hao-Ti Hung,^{4,5,‡}
Ying-Jer Kao,^{4,5,6,§} C.-J. David Lin,^{7,8,¶} and Amit Singh^{9,10,**}

¹*Max-Planck Institut für Quantenoptik, Garching 85748, Germany*

²*Munich Centre for Quantum Science and Technology (MCQST), Schellingstrasse 4, Munich 80799, Germany*

³*Faculty of Physics and Astronomy, Adam Mickiewicz University, Uniwersytetu Poznańskiego 2, 61-614 Poznań, Poland*

⁴*Department of Physics, National Taiwan University, Taipei 10617, Taiwan*

⁵*Center for Theoretical Physics, National Taiwan University, Taipei 10617, Taiwan*

⁶*Center for Quantum Science and Technology, National Taiwan University, Taipei 10617, Taiwan*

⁷*Institute of Physics, National Yang Ming Chiao Tung University, Hsinchu 30010, Taiwan*

⁸*Centre for High-Energy Physics, Chung-Yuan Christian University, Chung-Li 32023, Taiwan*

⁹*Department of Mechanical Engineering, National Yang Ming Chiao Tung University, Hsinchu 30010, Taiwan*

¹⁰*Department of Physics and Astronomy, University of Manchester, Manchester M13 9PL, United Kingdom*

Using tensor network methods, we simulate the real-time evolution of the lattice Thirring model quenched out of equilibrium in both the critical and massive phases and study the appearance of dynamical quantum phase transitions, as nonanalyticities in the Loschmidt rate. Although the presence of a dynamical quantum phase transition in the model does not correspond to quenches across the critical line of the equilibrium phase diagram at zero temperature, we identify a threshold in the energy density of the initial state, necessary for a dynamical quantum phase transition to be present. Moreover, in the case of the gapped quench Hamiltonian, we unveil a connection of this threshold to a transition between different regions in the finite-temperature phase diagram.

I. INTRODUCTION

Out-of-equilibrium dynamics is one of the most challenging problems in the study of quantum many-body systems. This funnels the interest towards finding universal behaviors that allow a more comprehensive understanding of the dynamics. A paradigmatic scenario to investigate these questions is that of a quantum quench [1], in which a system is evolved with a Hamiltonian of interest, after having been initialized in a certain (often pure) state. Since the mid-2010s, an active direction of research in this context has been the investigation of dynamical quantum phase transitions (DQPTs) [2, 3], which appear as zeros in the Loschmidt echo or return probability, i.e., the probability that the system is found in the initial state during the evolution.

One of the problems for studying out-of-equilibrium dynamics of such complex systems is the scarcity of appropriate tools. Only in certain cases is an analytical solution possible that allows a complete description of the time evolution after a quench [2, 4, 5]. For the most general cases, however, the only possibility is to obtain an approximation to the dynamics by means of numerical simulations, within the regimes where these are feasible. A relevant role among numerical methods is played by tensor network state (TNS) techniques [6–11]. In particular, in one-dimensional systems, matrix product state (MPS) [12–16] algorithms provide an effective way to explore the time-dependent properties of the Loschmidt echo

for systems in the thermodynamic limit [3, 17]. Although the potentially fast entanglement growth [18–20] limits the time that can be reliably simulated, TNS dynamical methods [21–23] enable an accurate picture of the quantity of interest for a moderate time after the quench, which has been exploited to obtain important results regarding DQPTs [17, 24–30].

Signatures of DQPT have been observed experimentally in trapped ion quantum simulators [31] and superconducting qubits [32]. While initial studies suggested that DQPTs occur when the parameter of the Hamiltonian is quenched across an equilibrium phase boundary [2, 3, 24], it was later realized that this is not the general case [17, 33–36], and the nature of DQPTs is more complex and far from being completely understood [29, 37].

The study of out-of-equilibrium physics for quantum field theories (QFTs), defined in the continuum, is highly nontrivial. Equilibrium properties of such models are usually addressed by the path integral formalism and Monte Carlo sampling, which, however, encounters a sign problem in certain scenarios. This limitation has motivated an investigation of applicability of TNS methods to the realm of QFT. In particular, gauge theories in 1+1 dimensions have been systematically addressed using TNS methods (see, e.g., Refs. [38–40] and references therein). Other QFTs and conformal field theories have also been studied in the same manner [41–44]. These investigations have focused on the equilibrium properties of the field theories. Real-time simulations are more scarce [45–49], and studying the real-time dynamics of a continuum QFT with these methods remains an open problem.

The most straightforward way to study QFT problems with TNS is to use the discretized version of the model Hamiltonian and apply standard TNS methods to find their equilibrium or dynamical properties. Such results depend on different lattice discretization schemes, but by repeating the procedure at

* banulsm@mpq.mpg.de

† krzysztof.cichy@gmail.com

‡ hunghaot1852@gmail.com

§ yjkao@phys.ntu.edu.tw

¶ dlin@nycu.edu.tw

** amitletit@gmail.com

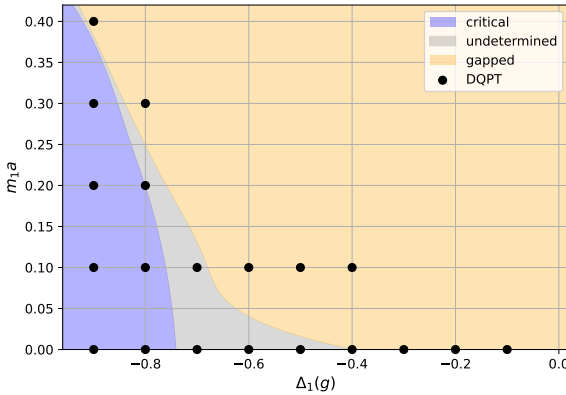


FIG. 1. Zero-temperature phase diagram of the Thirring model in the coupling-mass plane. The color-coded areas on the plot depict the equilibrium phase through correlator analyses [41]. The blue region is the critical region, where the constant C [defined in Eq. (9)] is less than 0.001; the orange region is the gapped phase region, where $C > 0.01$; the gray region is undetermined, where the corresponding $C \in [0.001, 0.01]$. The black point marks the location where we observe the DQPT, starting from the ground state of the Hamiltonian $H_1(m_1 a, \Delta_1)$ and quenching to $H_2(m_2 a = 0.1, \Delta_2 = 0.9)$.

different lattice spacings and performing the proper renormalization, it is possible to recover the continuum limit (see, e.g., Refs. [45, 50]). In this work, we focus on one such spin chain, corresponding to the discretization of the 1+1-dimensional Thirring model. The resulting spin model is a specialized XXZ Hamiltonian coupled to both staggered and homogeneous magnetic fields. The ground state of the model, as determined in previous work [41] using MPS, exhibits a critical and a gapped phase, separated by a Berezinskii-Kosterlitz-Thouless (BKT) phase transition (see Fig. 1). For vanishing bare fermion mass, the model is critical for all couplings.

In this work, we use uniform MPS to study the phenomenology of DQPTs in the spin model for the discretized Thirring model. We simulate quenches in both phases from initial states with very different properties. We show that a necessary condition for a DQPT to occur within the finite-time window that our numerical method can access is that the energy density of the initial state is above a certain threshold, independent of the phases of the initial and quenched Hamiltonian. However, in the case of the quench to the gapped phase we also identify a connection of DQPTs to the equilibrium phase diagram but at finite temperature. Namely, at the temperature corresponding to the identified energy density threshold, the properties of the thermal equilibrium state undergo a substantial change, with the vanishing of a string correlator that is nonzero in the ground state. We further show that the times at which DQPTs occur as a function of the energy density of the initial state show a structure reminiscent of the complex zeros of the Loschmidt amplitude [51, 52] and several branches of DQPTs that can be explored from different initial states.

The rest of the paper is structured as follows. In Sec. II we introduce the spin model that corresponds to the discretized Thirring Hamiltonian and present the MPS formulation and the tools and algorithms we have used. Second, we review the equilibrium phase structure of the Thirring model from the previous research in Sec. III. In Sec. IV, we discuss the DQPT concept and the use of MPS methods to study them in the model of interest. Our results for DQPTs in different quenches, and the relation of their appearance with the finite temperature phase diagram are discussed in Sec. V. Finally, in Sec. VI we summarize our findings and discuss potential further investigations.

II. FORMALISM

A. The Thirring model as a spin model

In this work we focus on the spin chain formulation corresponding to the lattice discretization of the massive Thirring model in 1+1 dimensions. The action of the original field theory is described by

$$S_{\text{Th}} [\psi, \bar{\psi}] = \int d^2x \left[\bar{\psi} i\gamma^\mu \partial_\mu \psi - m \bar{\psi} \psi - \frac{g}{2} (\bar{\psi} \gamma_\mu \psi)(\bar{\psi} \gamma^\mu \psi) \right], \quad (1)$$

where m is the fermion mass and g is the four-fermion coupling. To facilitate the use of MPS, quantization of the classical theory described by Eq. (1) is performed through the canonical method in the Hamiltonian formalism. One subtlety in this formalism is the inclusion of effects of the anomaly in the four-fermion operator. These effects can be easily investigated through the examination of the path-integral measure in the Lagrangian formulation [53]. In the canonical procedure, they need to be accounted for via a nonlocal definition of the currents in the four-fermion operator [54, 55].

The model can be discretized on a one-dimensional spatial lattice using the staggered regularization. For convenience of carrying out numerical computations in this work, the fermionic degrees of freedom in this Hamiltonian are mapped onto spin operators through the Jordan-Wigner transformation. Details of the above procedure can be found in Ref. [41]. Implementation of this strategy turns the Hamiltonian operator of the continuum Thirring model, H_{Th} , into that of the XXZ spin chain coupled to both uniform and staggered magnetic fields, up to a scaling factor,

$$\begin{aligned} H(\tilde{m}_0 a, \Delta) = & -\frac{1}{2} \sum_n^{N-2} (S_n^+ S_{n+1}^- + S_{n+1}^+ S_n^-) \\ & + a \tilde{m}_0 \sum_n^{N-1} (-1)^n \left(S_n^z + \frac{1}{2} \right) \\ & + \Delta(g) \sum_n^{N-1} \left(S_n^z + \frac{1}{2} \right) \left(S_{n+1}^z + \frac{1}{2} \right), \end{aligned} \quad (2)$$

where a is the lattice spacing, N is the total number of lattice sites, $S_n^\pm = S_n^x \pm iS_n^y$ and S_n^z are the spin matrices ($S_n^i = \sigma^i/2$ with σ^i being the Pauli matrices) at the n th site, and $[S_n^i, S_m^j]_{n \neq m} = 0$. Here $\tilde{m}_0 = m_0/\nu(g)$ with m_0 being the bare counterpart of the mass parameter, m , in Eq. (1). The functions $\nu(g)$ and $\Delta(g)$ are the lattice version of wavefunction renormalization and the four-fermion coupling [56],

$$\begin{aligned}\nu(g) &= \left(\frac{\pi - g}{\pi} \right) / \sin \left(\frac{\pi - g}{2} \right), \\ \Delta(g) &= \cos \left(\frac{\pi - g}{2} \right).\end{aligned}\quad (3)$$

Notice that the physical Hamiltonian is obtained by rescaling the dimensionless one in Eq. (2) by a factor $\nu(g)/a$. Throughout the rest of the paper, we will work with the lattice Hamiltonian (2) and correspondingly define dimensionless time and inverse-temperature parameters, which involve rescaling the physical (dimensionful) magnitudes by $\nu(g)/a$. Additionally, we restrict our consideration to the sector with total spin (magnetization) zero [41] and find the ground state by adding the penalty term (see Appendix A).

B. Matrix product state

A generic quantum state for a system of N spins can be written in the form

$$|\Psi_N\rangle = \sum_{\sigma_1, \dots, \sigma_N} c_{\sigma_1 \dots \sigma_N} |\sigma_1 \dots \sigma_N\rangle, \quad (4)$$

which can then be approximated as a MPS with bond dimension D ,

$$|\Psi_N\rangle = \sum_{\sigma_1, \dots, \sigma_N} \text{tr}[M_1^{\sigma_1} M_2^{\sigma_2} \dots M_N^{\sigma_N}] |\sigma_1 \dots \sigma_N\rangle, \quad (5)$$

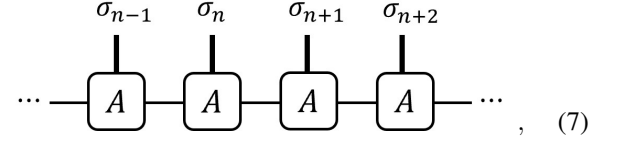
where $M_i^{\sigma_i}$ is a $D \times D$ matrix. For the open boundary condition, $M_1^{\sigma_1}$ and $M_N^{\sigma_N}$ become D -dimensional vectors. In this case, the trace in Eq. (5) becomes a simple product of matrices.

We search for DQPTs in the real-time evolution of Eq. (2). For this purpose, it is desirable to perform calculations directly in the thermodynamic limit. This can be accomplished by employing the uniform MPS (uMPS) technique, which allows for the description of the state of an infinite spin chain with translation invariance using one bulk tensor and two appropriate boundary tensors [57, 58]. The uniform MPS can be represented as

$$|\Psi(A)\rangle = \sum_{\sigma} (\dots A^{\sigma_{n-1}} A^{\sigma_n} A^{\sigma_{n+1}} A^{\sigma_{n+2}} \dots) |\sigma\rangle, \quad (6)$$

where $A^{\sigma_n} \in \mathbb{C}^{D \times D}$ for $\sigma = 1, \dots, d$. It can be represented

diagrammatically as



where A is the unit cell of the uMPS. Due to the staggered term in Eq. (2), the system is translationally invariant with a period of two. Thus, we choose the tensor A to represent two contiguous sites of the chain, and its physical dimension becomes $d = 4$.

III. EQUILIBRIUM PHASE STRUCTURE OF THE 1+1-DIMENSIONAL THIRRING MODEL

In this section, we review our study of the zero-temperature phase structure of the Thirring model using MPS [41]. An analysis of renormalization group (RG) equations of the dual sine-Gordon theory [59–61] points to the existence of two phases in the Thirring model. The massless theory is a conformal field theory at all couplings $\Delta(g)$. RG flows in the mass-coupling plane reveal that the line $m = 0$ is a fixed line under RG transformations. However, it is stable/unstable for couplings $\Delta(g)$ below/above certain $\Delta(g_*)_m = -\pi/2$. At $m > 0$, the nonzero fermion mass is an irrelevant operator for $\Delta(g) < \Delta(g_*)_m$ but becomes relevant when $\Delta(g) > \Delta(g_*)_m$, with the transition coupling $\Delta(g_*)_m$ being mass dependent. This gives rise to two equilibrium phases:

- (i) $\Delta(g) < \Delta(g_*)_m$: gapless (critical) phase
- (ii) $\Delta(g) > \Delta(g_*)_m$: gapped (massive) phase,

separated by a BKT transition. The BKT transition was originally discussed in the context of the XY model [62, 63], which is actually dual to the sine-Gordon and Thirring theories, with the XY model temperature dual to the couplings of these theories. For a more extensive discussion of these aspects, including von Neumann entanglement entropy and chiral condensate, we refer to Ref. [41].

The quantitatively most robust analysis of the phase structure and the determination of $\Delta(g_*)_m$ is about the string correlator,

$$\begin{aligned}C_{\text{string}}(x) &= \frac{1}{N_x} \sum_n \langle S^z(n) S^z(n+1) \dots \\ &\quad \dots S^z(n+x-1) S^z(n+x) \rangle,\end{aligned}\quad (8)$$

which is a string of S^z operators. We note that Ref. [41] erroneously states this string correlator as the fermion-antifermion one, containing $\langle S^+(n) S^z(n+1) \dots S^z(n+x-1) S^-(n+x) \rangle$ terms. At large-enough distances, the correlator $C_{\text{string}}(x)$ exhibits a power-law decay in the gapless phase, given by $C_{\text{string}}(x) \propto \beta x^{-\alpha}$, and a power-exponential decay in the gapped phase, $C_{\text{string}}(x) \propto B x^{-\eta} A^x$. The crucial distinction that makes the string correlator particularly useful for determining $\Delta(g_*)_m$ is that it decays to a constant, C , in the

gapped phase. In practice, one can analyze both phases based on the power-exponential fitting ansatz:

$$C_{\text{string}}(x) = Bx^{-\eta}A^x + C, \quad (9)$$

with $A = 1$ found in fits in the gapless phase. Thus, the phase transition when going from the gapless into the gapped phase is manifested by A dropping below 1 and, in the case of the string correlator, by $C > 0$. The onset of the nonzero constant is numerically more robust than the smooth drop of A below 1, accounting for the practical usefulness of the string correlator. As we will see below, this is true also at nonzero temperatures and it will allow us to identify relations between thermal phases of the Thirring model and DQPTs.

As a summary of our findings for the zero-temperature phase structure, we show Fig. 1. The color-coded regions correspond to the equilibrium phase on the coupling-mass plane through the correlator analyses from our previous work [41]. In particular, we fitted Eq. (9) and extracted values of the constant C . Since the results depend, in general, on the fitting interval, we adopted a systematic procedure to assess the systematic uncertainty of C (dominating with respect to other uncertainties, coming from the finite bond dimension and the finite volume). For details of this procedure, we refer again to Ref. [41]. Depending on the value of C , we identified three situations. With $C < 0.001$ or $C > 0.01$, one unambiguously concludes either the critical phase (purple region) or the gapped phase (orange region), respectively. If $C \in [0.001, 0.01]$ (gray region), then the systematic uncertainty does not allow us to draw conclusions about a (non)vanishing value of C . This region of ambiguous values of C is indicated by gray shading and the BKT transition must occur there. We note the onset a nonzero value of C is very smooth at small fermion masses, while it becomes rather sharp with an increasing mass. At very small masses, the implied transition point is consistent with the RG flow analysis [$\Delta(g) \approx -\pi/2$] and at large masses, it moves towards more negative values.

IV. THE LOSCHMIDT ECHO AND THE MIXED TRANSFER MATRIX

A. Quantum quench and DQPT

In this work, we investigate DQPT in a quantum quench. A quantum quench is the paradigmatic scenario where to study nonequilibrium dynamics of a quantum system. The system is assumed to be prepared in a certain initial state $|\Psi_1\rangle$, typically the ground state of a Hamiltonian H_1 . From time $t = 0$ on, it is evolved with a different Hamiltonian H_2 . The evolved state can be written as $|\Psi(t)\rangle = e^{-itH_2}|\Psi_1\rangle$. The key ingredient in the study of DQPT is the Loschmidt amplitude,

$$G(t) = \langle\Psi_1|\Psi(t)\rangle = \langle\Psi_1|e^{-itH_2}| \Psi_1\rangle, \quad (10)$$

which is analogous to the boundary partition function [64] $Z_B(z) = \langle\Psi_1|e^{-zH_2}|\Psi_1\rangle$ in the complex plane $z \in \mathbb{C}$.

The nonanalytical points of the free energy density $f(z) = -\lim_{N \rightarrow \infty} \frac{1}{N} \log Z_B(z)$ are believed to indicate phase transitions [65]. The squared modulus of Loschmidt amplitude in Eq. (10), the Loschmidt echo, quantifies the return probability, i.e., the probability of the system being found in the initial state after a certain time t . In the thermodynamic limit ($N \rightarrow \infty$), the Loschmidt echo will approach $e^{-Nr(t)}$, with the rate function

$$r(t) = -\lim_{N \rightarrow \infty} \frac{1}{N} \log |G(t)|^2. \quad (11)$$

This function can be interpreted as a dynamical free energy, and can exhibit nonanalyticities. DQPTs are defined as the times when $r(t)$ is nonanalytical [2]. In some cases, DQPTs are associated with quenches across an equilibrium phase transition [2, 66], but such connection to equilibrium is not always present [33], which motivates the identification of DQPTs as a genuinely nonequilibrium effect. The potential observable signature of DQPTs in local and string quantities has also been a subject of intensive studies. [67, 68] The complex phenomenology of DQPTs has motivated studies in multiple models, but the phenomenon is yet far from a full theoretical understanding [3, 17, 27, 69, 70].

The transfer matrix formalism allows for a systematic exploration of the character of DQPTs [17, 25–27, 29]. We focus here on the case where the initial state is a MPS and consider directly the translationally invariant case, i.e., the initial state is parametrized by a single rank-3 tensor A . The Loschmidt amplitude, for a translationally invariant system of N sites, can then be expressed as

$$G(t) = (l|T^N(t)|r) = \lambda_0^N, \quad (12)$$

where $T(t)$ is the mixed transfer matrix defined by

$$T(t) := \sum_i \bar{A}(0)^\sigma \otimes A(t)^\sigma, \quad (13)$$

and $A(t)$ represents the tensor describing the evolved state. The vectors $(l|$ and $|r)$ are the left and right eigenvectors with the leading eigenvalue λ_0 , satisfying $(l|r) = 1$. Graphically,

$$T(t) = \begin{array}{c} \text{---} \bar{A}(0) \text{---} \\ | \qquad \qquad \qquad | \\ \text{---} A(t) \text{---} \end{array}. \quad (14)$$

The Loschmidt rate is thus determined by the spectrum of the (in general non-Hermitian) matrix $T(t)$ and, in the thermodynamic limit, by its dominant eigenvalue $\lambda_0(t)$. DQPTs appear when there is an eigenvalue crossing and the eigenvector associated to the dominant eigenvalue changes [17, 71].

B. Investigation of DQPT in the lattice version of the Thirring model

Here we focus on the Hamiltonian Eq. (2) and consider quenches from the ground state $|\Psi_1\rangle$ of the model with a

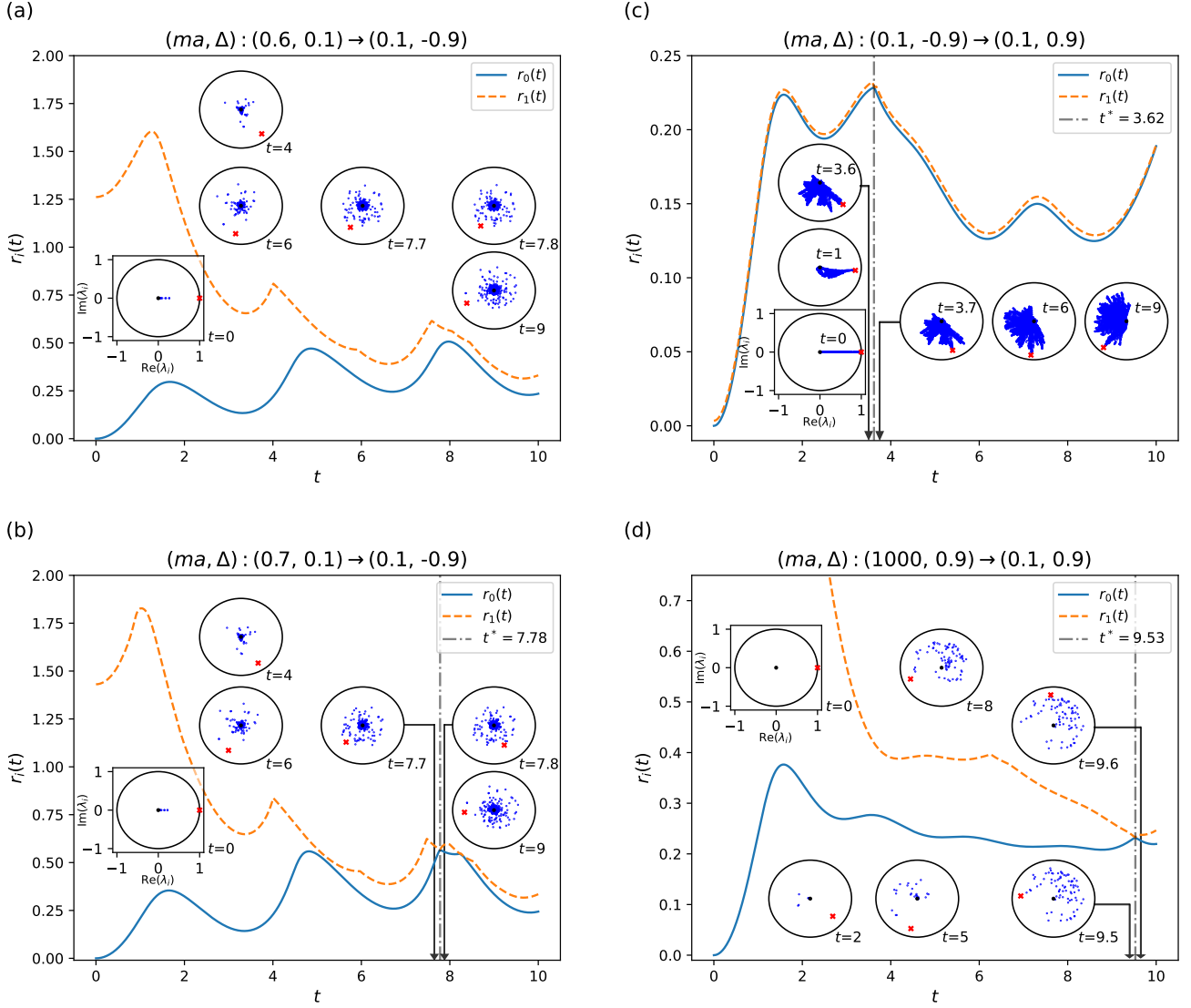


FIG. 2. The return rate function and the full spectrum of the mixed transfer matrix $T(t)$. The quantity r_i is defined in Eq. (15), while r_0 corresponds to the return rate function defined in Eq. (11). The insets display the full spectrum of the mixed transfer matrix $T(t)$ defined in Eq. (14), with the red cross representing the corresponding dominant eigenvalue. The time t^* (indicated by the gray dash-dotted line) denotes when the first DQPT occurs. This plot shows how the nonanalyticities in the return rate $r_0(t)$ correspond to discontinuous jumps in the phase of the dominant eigenvalue of $T(t)$ (red point). We can notice that in (a), with $(m_1 a, \Delta_1) = (0.6, 0.1)$ and $(m_2 a, \Delta_2) = (0.1, -0.9)$, there are no DQPTs. However, in (b), a small increase in $m_1 a$ to 0.7, with the same quench Hamiltonian, induces a DQPT at $t^* = 7.78$.

given set of parameters, $H_1 = H(m_1 a, \Delta_1)$. The quench Hamiltonian, with which the state is evolved, will be denoted as $H_2 = H(m_2 a, \Delta_2)$. For a fixed H_2 , we study the real-time evolution of different initial states, $|\Psi_1\rangle$. The latter are represented by their MPS approximation, obtained using the variational uMPS (VUMPS) algorithm [58], and the real-time evolution according to H_2 can be numerically simulated using a standard tensor network algorithm [7, 11, 72]. In particular, we use time-dependent variational principle (TDVP) algo-

rithm [21, 73] to obtain the time-dependent tensors of the MPS representation, $A(t)$. We obtain the spectrum of the mixed transfer matrix, $T(t)$, using Eq. (13) and explore the appearance of DQPTs for various quench parameters. To investigate how DQPTs occur, we introduce the following quantity:

$$r_i(t) = -\log |\lambda_i(t)|^2, \quad (15)$$

where $\{\lambda_i\}$ is the spectrum of the mixed transfer matrix $T(t)$, satisfying $|\lambda_0| \geq |\lambda_1| \geq \dots$. Notice that r_0 is exactly return

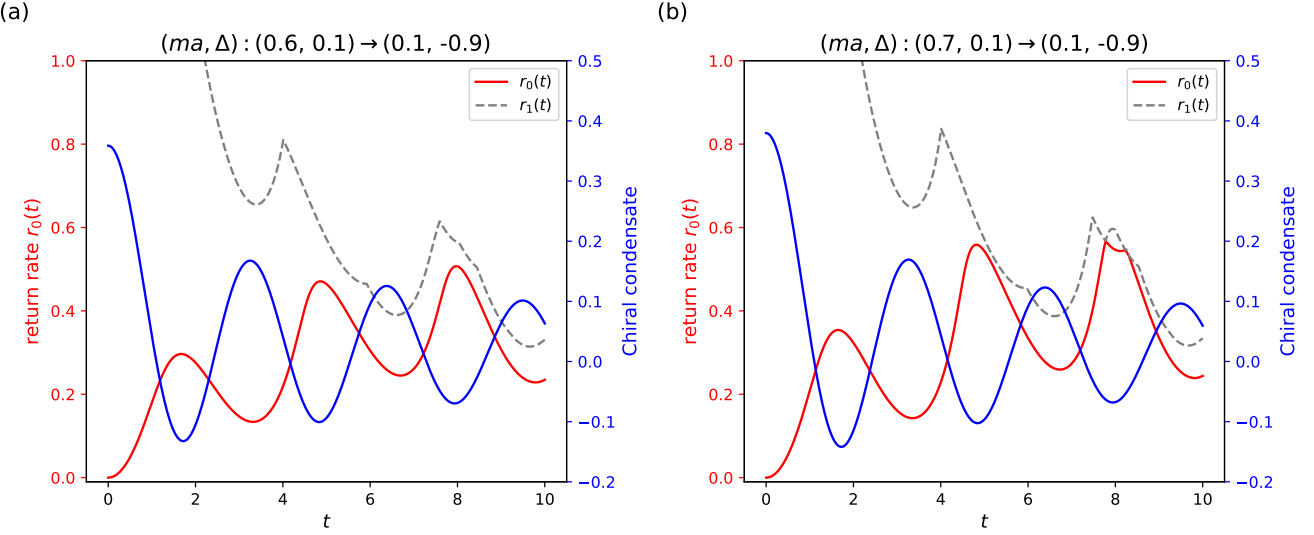


FIG. 3. The return rate functions (red) and the chiral condensate (blue) for the cases (a) without and (b) with DQPTs. The parameters we choose here are the same as those in Figs. 2(a) and 2(b).

rate function defined in Eq. (11). Figure 2 shows the results for a selection of simulation parameters. The first DQPT occurs when $t = t^*$. The insets show snapshots of the spectrum of $T(t)$, which demonstrate that the nonanalytical points in the return rate function in Eq. (11) are associated with a discontinuous jump in the phase of the dominant eigenvalue of this mixed transfer matrix [71].

By choosing parameters, $(m_1 a, \Delta_1)$ and $(m_2 a, \Delta_2)$, to be in a different or in the same equilibrium phase, we can simulate quenches across the phase diagram, which we determined in our previous study [41]. We find that, as observed in other models [17, 33], the equilibrium phases of H_1 and H_2 does not determine the presence of DQPTs, which can appear in both types of scenario. In Fig. 1, we illustrate that the existence of DQPTs is not equivalent to the equilibrium phase. DQPTs have been demonstrated to occur in quenches that happen entirely within either of the equilibrium phases.

C. DQPT and thermalization

Notice that DQPTs and (pre-)thermalization happen at different timescales. In our setup, DQPTs can occur at relatively short times. Hence, we do not expect that local observables have equilibrated yet. Indeed, we observe that local observables are still varying strongly at the time slices when the DQPTs are observed. To illustrate this, we plot in Fig. 3 the time evolution of the chiral condensate (or the staggered magnetization in spin model language),

$$\chi \sim \frac{1}{N} \left| \sum_n (-1)^n \left(S_n^z + \frac{1}{2} \right) \right|,$$

in both the cases with or without DQPT. The chiral condensate shows strong time variation at the longest time allowed for our simulation, $t = 10$, in both cases, indicating DQPT and prethermalization or thermalization phenomena occur at different timescales.

V. DQPTS AND FINITE-TEMPERATURE PHASE DIAGRAM

A. Energy threshold and the inverse temperature

As discussed in the previous section, the appearance of a DQPT after a certain quench is not determined by the fact that the quench crossed an equilibrium phase boundary. Hence the ground state of H_2 is not the most adequate equilibrium reference for all initial states. Since the mean energy of the initial state $E_1 := \langle \Psi_1 | H_2 | \Psi_1 \rangle$ is typically much higher than the ground-state energy of the quench Hamiltonian H_2 , one does not necessarily expect the time-evolved state to be close to the ground state of H_2 , even at the level of local observables. Instead, it is more meaningful to compare the local properties to those of the thermal equilibrium state at the same energy density. If the system equilibrates (in the sense of locally resembling an equilibrium ensemble), then the thermal state should correspond to the maximal entropy state compatible with the conserved quantities [74]. Our particular model conserves energy and total magnetization, and we are considering initial states in which the latter vanishes. Thus, the relevant equilibrium state is the Gibbs state with the same energy E_1 , restricted to the subspace of vanishing total magnetization; namely (and up to normalization) $\rho(\beta) \propto P_{s_z=0} e^{-\beta H_2} P_{s_z=0}$, where $P_s = \sum_{n, S_z|n\rangle=s|n\rangle} |n\rangle\langle n|$ is the

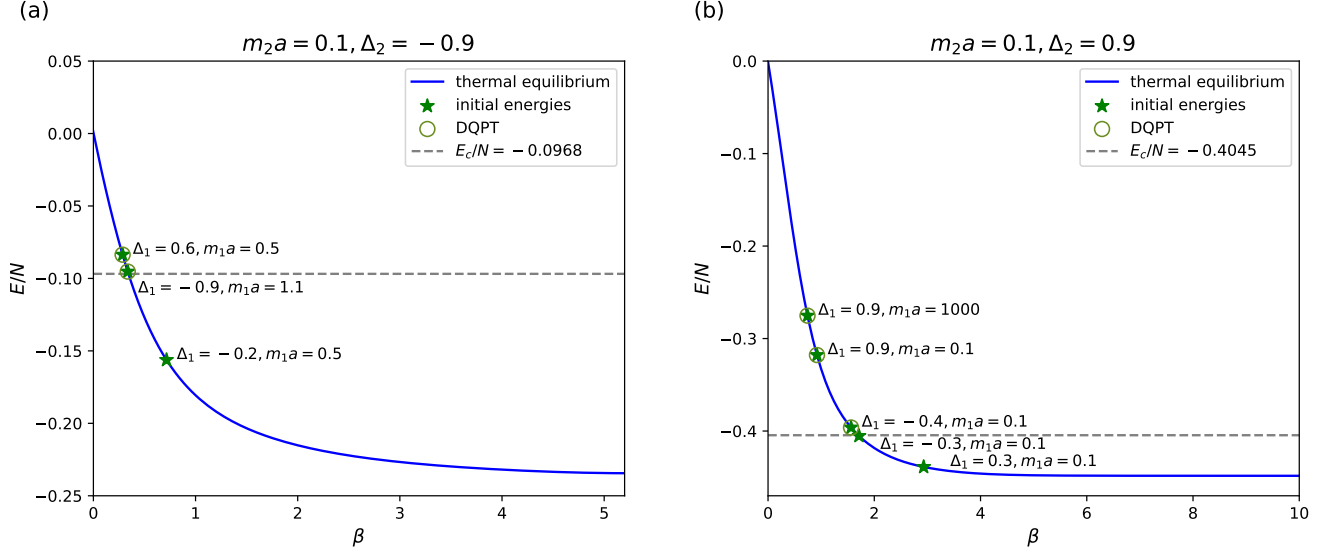


FIG. 4. Relation $E(\beta)$ between the mean energy and the inverse temperature in the Gibbs state restricted to the zero magnetization sector for $(m_2a, \Delta_2) = (0.1, -0.9)$ (left:critical phase) and $(0.1, 0.9)$ (right:gapped phase). We display the energy densities of several explored quenches using star symbols, and circles indicate the initial states where our simulations reveal the occurrence of at least one DQPT. Additionally, the dashed line denotes the lowest value of energy density (E_c/N) at which a DQPT was observed (see also Fig. 5). For $(m_2a, \Delta_2) = (0.1, -0.9)$ (left), $E_c/N = -0.0968$ and the corresponding inverse temperature $\beta_c \approx 0.34$; for $(m_2a, \Delta_2) = (0.1, 0.9)$ (right), $E_c/N = -0.4045$ and $\beta_c \approx 1.70$.

projector onto the sector of total magnetization s . The inverse temperature $\beta_1 := \beta(E_1)$ corresponding to the state is fixed by the condition

$$E_1 = E(\beta_1) := \frac{\text{tr}(\rho_{\beta_1} H_2)}{\text{tr}(\rho_{\beta_1})}. \quad (16)$$

The determination of β_1 can be achieved using standard TNS methods, exploiting the fact that the thermal equilibrium state for a local Hamiltonian can be approximated efficiently by a matrix product operator (MPO) [75, 76]. More concretely, given a value of the inverse temperature β , the canonical purification of the thermal equilibrium ensemble restricted to the vanishing magnetization sector can be written as $|\Psi(\beta)\rangle := e^{-\beta H_2/2} \sum_{n, S_z|n\rangle=0} |n\rangle_S |n\rangle_A$, where the sum runs over a basis restricted to the sector $S_z = 0$, and the subscripts S and A refer respectively to the system and ancillary degrees of freedom. This state, also known as thermofield double state, can be approximated by a MPS using standard tensor network algorithms [6, 7]. This is achieved by preparing a maximally-mixed state of the system and the ancilla, expressed as a simple MPS, where each system site is entangled only with one, next neighbor, ancillary site, and evolving it in imaginary time with an approximation of the operator $e^{-\beta H_2/2}$. In order to restrict the ensemble to a sector of fixed magnetization, we write the projector onto the sector $S_z = 0$ as a MPO and use as initial mixed state, instead of the identity. Additionally, this MPO can also be applied to the intermediate state during the evolution to ensure that truncation errors due to the approximations do not induce undesired magnetization components. For a finite system of size N , the projector

onto vanishing magnetization has an exact MPO representation, with bond dimension $N/2$. Applying the aforementioned TNS evolution algorithm in imaginary time to the vectorized projector provides a MPS approximation to $|\Psi(\beta)\rangle$ for varying β , from which the thermal expectation value of a physical observable O can be computed directly as

$$\langle O \rangle_\beta := \frac{\text{tr}(O \rho_\beta)}{\text{tr} \rho_\beta} = \frac{\langle \Psi(\beta) | O \otimes \mathbb{I} | \Psi(\beta) \rangle}{\langle \Psi(\beta) | \Psi(\beta) \rangle}, \quad (17)$$

where the second factor in the tensor product is the identity acting on the ancillary system. In particular, computing the energy along the imaginary time evolution provides an estimate of the function $E(\beta)$, from which we can extract the value β_1 corresponding to a given initial state by inverting it numerically.

For concreteness, in the rest of the section we focus on two quenches, corresponding to Hamiltonians in each of the phases (see Fig. 1). Here we choose $(m_2a, \Delta_2) = (0.1, -0.9)$ in the gapless phase and $(m_2a, \Delta_2) = (0.1, 0.9)$ in the gapped one. For each of them we approximate the thermal equilibrium state in a system of $N = 300$ sites, sufficiently large to neglect finite-size effects in this analysis. The corresponding $E(\beta)$ curves are shown in Fig. 4.

For each of the simulated initial states, we can now extract the effective temperature from these curves. The ground states of the different initial Hamiltonians H_1 correspond to initial states with different effective temperatures. Since the latter only depends on the energy E_1 , states in very distant regions of the equilibrium phase diagram may have the same temperature. As an illustration, we show the energy densities of some

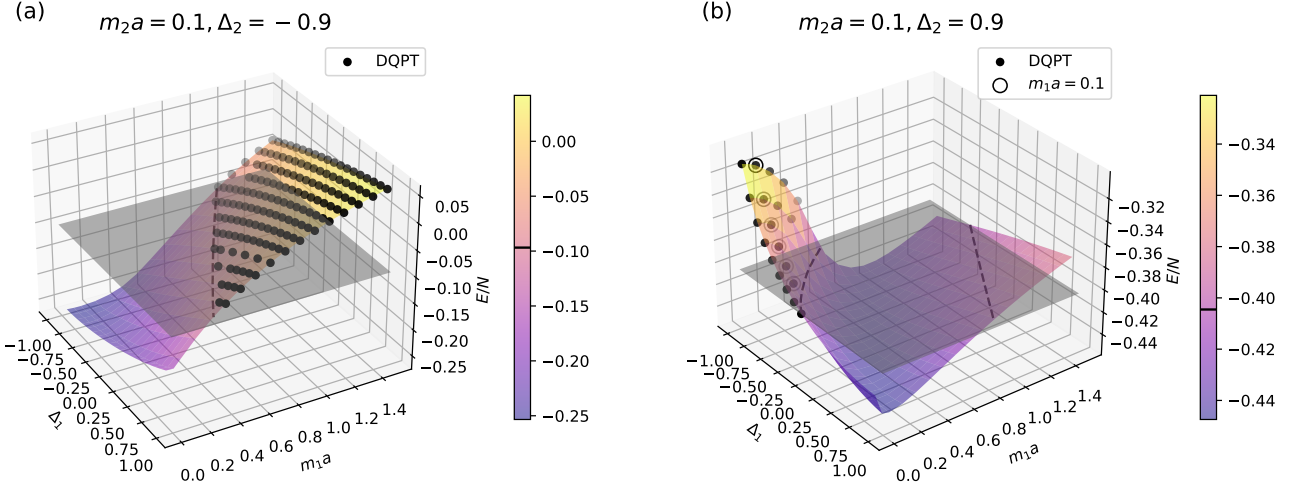


FIG. 5. Energy densities corresponding to ground states of varying m_1a and Δ_1 , as a function of these parameters, for the quench to the critical phase ($m_2a = 0.1$, $\Delta_2 = -0.9$) (left) and the gapped phase ($m_2a = 0.1$, $\Delta_2 = 0.9$) (right). In each case, the dots indicate where DQPT has been observed. The horizontal plane shows the energy threshold, E_c/N , which is also marked as a black line on the color bars. On the right panel, the circles indicate the family of quenches from constant $m_1a = 0.1$.

of the explored quenches with star symbols in Fig. 4. We furthermore indicate with circles the initial states for which our simulations show the appearance of (at least one) DQPT. From these results we observe that for DQPTs to be present, the effective temperature of the initial state needs to surpass a certain threshold. This seems to suggest that a decisive factor for the occurrence or not of a DQPT is the amount of excitation energy in the initial state.

To verify this observation, we estimated the value of E_1 for a grid of (m_1a, Δ_1) values, $0 < m_1a \leq 1.5$ and $-1 \leq \Delta_1 \leq 1$, and identified the regions of parameters for which the threshold (denoted as E_c) is surpassed (see Fig. 5). We conducted this study for both quench Hamiltonians mentioned above. For the gapless Hamiltonian, $(m_2a, \Delta_2) = (0.1, -0.9)$, the value of E_1 increases smoothly with both m_1a and Δ_1 , and the plane of constant $E_c/N \approx -0.0968$, corresponding to the lowest value for which a DQPT was observed. As indicated in Fig. 5(a), this divides the parameter space in two connected regions. Consistent with this, we find DQPTs for all initial states sampled from the region with higher energy.

In contrast, for the quench into the gapped phase, $(m_2a, \Delta_2) = (0.1, 0.9)$, the dependence of E_1 on (m_1a, Δ_1) is not monotonic. We find two disjoint regions of parameters with energies above the identified threshold $E_c/N \approx -0.4045$, lying on opposite corners of the parameter space as can be seen in Fig. 5(b). One region with negative Δ_1 and small m_1a (overlapping but not coinciding with the critical phase, as shown in Fig. 1), and the other region with positive large Δ_1 and m_1a , deep within the gapped regime. We simulate quenches from both regions, as well as interme-

iate parameters with energy E_1 below the threshold. For the first high-energy region, i.e., negative Δ_1 and small m_1a , we consistently observe DQPTs for energies above the threshold. The second region, with large positive Δ_1 and m_1a , however, seems to exhibit DQPTs only at much later times than the first. An extreme case is shown in Fig. 2(d), for the quench from $m_1a = 1000$, $\Delta_1 = 0.9$, for which we observe a DQPT only close to $t \approx 10$. We observe that as m_1a values decrease, the time at which the first DQPT is observed increases even more, so that we need to run long-time simulations to analyze this region. Due to limitations imposed by truncation errors, we can reliably explore times up to only $t \lesssim 14$. Within this window, we only observe DQPTs for points in the parameter regime with masses outside our original grid. We presume that longer times would identify DQPTs also in the rest of the region above the threshold.

This exploration of the parameter space indicates that for states with similar effective temperature, but corresponding to very different values of (m_1a, Δ_1) , the DQPTs may occur in very different ways. In order to obtain a more complete picture, we plot in Fig. 6, the times at which we observe DQPTs as a function of the effective temperature of the initial state for all the simulated cases. For each of the initial states, we determine β from the energy expectation value $\langle \Psi_1 | H_2 | \Psi_1 \rangle$ through Eq. (16). The figure shows not only the first observed nonanalyticity (blue dots), but the times of all subsequently observed DQPTs (with colors indicating the number of the DQPT). These figures are reminiscent of the nonanalyticities shown by the complex Loschmidt rate, when defined on the complex t plane for a fixed initial state [3]. In such case, the nonanalyticities of the rate in the complex-time

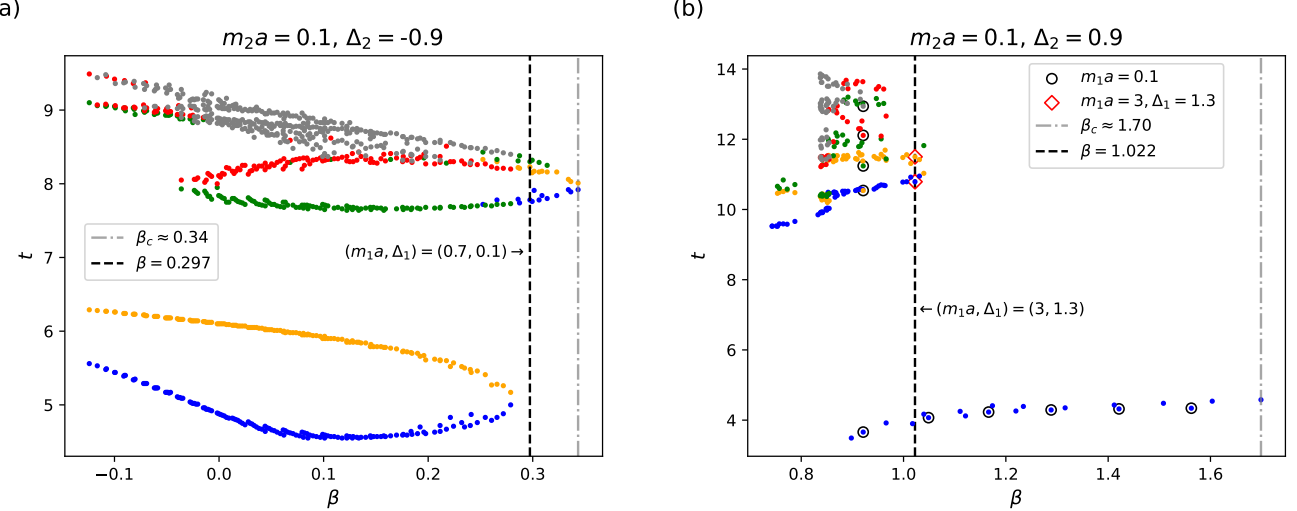


FIG. 6. The DQPTs on the inverse temperature–time plane. The first, second, third, and fourth occurrences of DQPTs are colored blue, orange, green, and red, respectively. Gray indicates occurrences beyond the fourth. The gray dash-dotted line denotes the critical inverse temperature β_c . (a) We simulate the evolution parameters $m_2a = 0.1$ and $\Delta_2 = -0.9$ (critical phase) and perform a scan for the initial parameters ($m_1a = 0.1, 0.2, \dots, 1.5; \Delta_1 = -0.9, -0.8, \dots, 0.9$). For example, the dashed line is the case for $m_1a = 0.7$ and $\Delta_1 = 0.1$, which is also specifically shown in Fig. 2(b). (b) The simulation results for the evolution parameters $m_2a = 0.1$ and $\Delta_2 = 0.9$ (gapped phase), scanning for the initial parameters as follows: $(m_1a = 0; \Delta_1 = -0.9, -0.8, \dots, -0.1, 0.9)$, $(m_1a = 0.1, 0.2, \dots, 1.5; \Delta_1 = -0.9, -0.8, \dots, 0.9)$, $(m_1a = 1, 2, \dots, 9; \Delta_1 = 1, 1.1, 1.3, 1.5, \dots, 1.9)$, and $(m_1a = 10, 20, 30, 40, 60, 80, 100, 1000; \Delta_1 = 0.9)$. These large masses are chosen to explore the large Δ_1 , large m_1a corner of Fig. 5(b), while ensuring that DQPT occurs within our simulation window ($t < 14$). The black dashed line and the red diamond symbols represent the case for $m_1a = 1.3$ and $\Delta_1 = 3$, where DQPT does not occur at the lowest branch near $t \approx 4$.

plane are analogous to Fisher zeros of a boundary partition function and determine the presence and time of occurrence of DQPTs [51, 52]. In our case, the initial state varies and we do not evolve it in imaginary time, but the results suggest that our effective temperature does play an equivalent role, allowing us to explore such complex plane from purely real-time data. However, we also observe that some initial states are not sensitive to some of the DQPT *branches*. For instance, if we select $(m_1a, \Delta_1) = (3, 1.3)$ and quenches to $(m_2a, \Delta_2) = (0.1, 0.9)$ [indicated by the black dashed line and red diamond marks in Fig. 6(b)], then the DQPT does not occur at the lowest branch near $t \approx 4$. The generality of this connection for other models thus needs further investigation.

B. String correlator and DQPT

Some DQPTs have been connected to equilibrium phase diagrams [2, 3, 24, 77]. In Ref. [41], we identified the ground-state phase structure by analyzing the behavior of the string correlator (8) (see Sec. III). Namely, the zero-temperature gapless phase is characterized by the string correlator decaying to zero at large distances ($C = 0$), while the gapped phase evinces a decay of this correlator to a nonzero value ($C > 0$). In the present work, we use similar methodology to connect the occurrence of DQPT to the thermal string correlator, pertaining to the effective temperature of the initial state. As in Ref. [41], we fit the distance-dependent string correlators with

the power-exponential ansatz given by Eq. (9). To establish the connection to DQPT, we note that, keeping the mass fixed, $m_1a = m_2a = 0.1$, and varying Δ_1 , each value of the coupling corresponds to a different effective β , as illustrated in Fig. 4(a) (for $\Delta_2 = -0.9$) and Fig. 4(b) (for $\Delta_2 = 0.9$).

We start the discussion with the latter, $\Delta_2 = 0.9$. We observe the following correspondence (see also Fig. 7):

(i) for $\beta \leq 1.563$ ($\Delta_1 \leq -0.4$), the constant C is consistent with zero [at $\beta = 1.563, C = 0.000004(4)$] and DQPT is observed,

(ii) for $\beta \geq 1.712$ ($\Delta_1 \geq -0.3$), a nonzero constant emerges [at $\beta = 1.712, C = 0.000046(10)$] and we find no DQPT.

The observed correspondence pertains to DQPTs pictured in the lowest branch of Fig. 6(b), explicitly marked with circles when $m_1a = m_2a$. Thus, this kind of DQPT is related to a substantial change in the properties of the thermal state, characterized by a different value of C . The former/latter may be the thermal counterpart of the zero-temperature critical/gapped phase, but a detailed characterization of finite-temperature phases of the model is beyond the scope of our work.

The picture is somewhat different for $\Delta_2 = -0.9$. In this case, $C = 0$ at all temperatures, regardless of the occurrence of DQPT, found at $\beta \lesssim 0.34$ [see Fig. 6(a)]. Note, however, that none of the DQPTs represented in Fig. 6(a) occur at $m_1a = m_2a$, i.e., a prerequisite for DQPT at $\Delta_2 = -0.9$ is to have a quench in fermion mass. Thus, for the final Hamil-

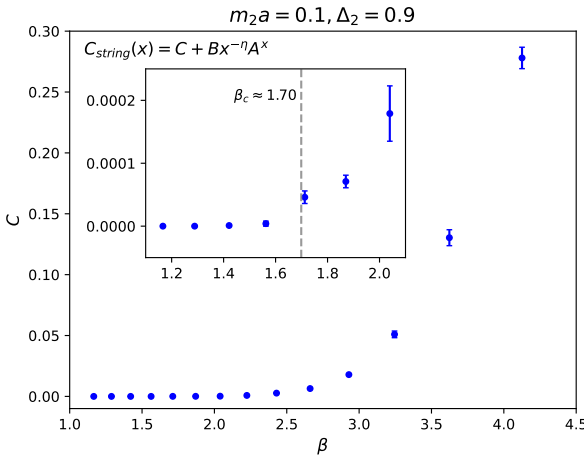


FIG. 7. Value of the constant C , defined in Eq. (9), that characterizes the long-distance behavior of the string correlator (8) for the thermal equilibrium state of the Hamiltonian $(m_2a, \Delta_2) = (0.1, 0.9)$ as a function of the inverse temperature β . The gray dashed line in the inset denotes the critical inverse temperature β_c .

tonian in the critical phase $(m_2a, \Delta_2) = (0.1, -0.9)$, the analyzed string correlator does not exhibit a similar correlation to the presence of DQPTs as the one observed for the quench into the gapped Hamiltonian. This might be understood because the asymptotic value of the string correlator detects the order present in the ground state of the gapped phase, which is destroyed as the temperature (energy) increases, whereas the ground state in the critical case does not exhibit such order. On the other hand, the DQPT threshold detected by the correlator in the gapped quench corresponds to the abrupt edge of the lower DQPT branch in Fig. 6(b), a feature that does not appear either in the corresponding Fig. 6(a) for the critical quench. Although we conclude that the thermal string correlators defined in Eq. (8) are not universal indicators for the possibility of DQPTs, a more detailed investigation is needed to fully characterize which DQPTs are associated to changes in these quantities and to determine whether other thermal observables can detect the different boundaries of DQPT branches observed in Fig. 6. We thus leave the investigation of finite-temperature phases and their potential relation to DQPTs for future work.

VI. CONCLUSION

Using standard TNS methods, we have investigated the occurrence of DQPTs in the lattice discretization of the Thirring model, which corresponds to a spin-1/2 XXZ chain coupled to a uniform and a staggered magnetic field, with two free dimensionless parameters, respectively related to the coupling and the mass. Using the uniform MPS ansatz to work directly in the thermodynamic limit, we have simulated quenches where the evolution is given by a constant Hamiltonian and

the initial state is chosen as the ground state for different parameters, in the same or a different phase. We then studied the time evolution of the spectrum of the mixed transfer operator, whose dominant eigenvector directly determines the Loschmidt rate. DQPTs are found when another eigenvalue crosses with the largest one.

We have identified a threshold in the energy density of the initial state below which DQPTs do not occur, at least during the finite times reachable by our simulations. The threshold is observed both for quenches in the gapless and the gapped phases. The energy density of each initial state corresponds to an effective temperature: that of the thermal equilibrium state with the same energy per spin, restricted to the sector of zero magnetization. This thermal state is the one expected to describe the equilibrium values of local observables after the quench in the long-time limit, since energy and magnetization are the only local conserved quantities in the problem.

We have analyzed the position of each observed DQPT (or nonanalyticity of the Loschmidt rate) in the time-effective-temperature plane. This reveals structures of nonanalyticities reminiscent of the zeros in the complex-time plane of the Loschmidt rate defined for a fixed initial state. Our results show that DQPTs for different initial states lie in multiple well-defined branches. Initial states in different phases can appear on the same branch, which thus is not related to the zero-temperature phase diagram. All DQPT branches start at some minimal effective temperature. In most cases, the lowest temperature edge of a branch corresponds to a smooth merge with another one. However, in the case of the quench with the gapped Hamiltonian, we identify a particular branch, with DQPTs happening at the shortest times, with a sharp end at $\beta_c \sim 1.7$. We have found that this energy threshold corresponds very accurately with a substantial change in the properties of the thermal equilibrium states at the corresponding effective temperature. More concretely, below this temperature, a certain string correlator attains a nonzero value at long distances, a property that also characterizes the ground state in the gapped phase. For this branch, we have thus established a relation between the presence of DQPTs and the equilibrium phase diagram at finite T . We have not found a similar correspondence for the smooth thresholds of branches that merge into each other.

Our study thus suggests that observing the dynamics and analyzing the DQPTs from different initial states can probe properties of the finite-temperature phase diagram, in particular when a sharp threshold is found for the occurrence of these nonanalyticities. Since our simulations are limited to finite-time windows, due to the accumulation of truncation error, and we have not mapped out the complete thermal equilibrium properties at all temperatures, further investigation is needed to determine whether the other observed branches correspond also to some quantifiable equilibrium property. It is also interesting to investigate whether similar effects appear in other spin models, and the precise correspondence between Fisher zeros and the DQPT lines in our time-effective temperature representation.

ACKNOWLEDGMENTS

The authors thank I. McCulloch, L. Tagliacozzo, M. Fagotti, L. Barbiero, and N. Cuzzuol for very useful discussions. This work was partly supported by the DFG (German Research Foundation) under Germany's Excellence Strategy – EXC-2111 – 390814868 and Research Unit FOR 5522 (Grant No. 499180199) and by the EU-QUANTERA project TNiSQ (BA 6059/1-1), as well as Taiwanese NSTC Grants No. 110-2112-M-002-034-MY3, No. 112-2112-M-A49-021-MY3, No. 112-2119-M-007-008, and No. 113-2119-M-007-013. Numerical computations were performed on HPC facilities at National Taiwan University and National Yang Ming Chiao Tung University.

DATA AVAILABILITY

The data and code to generate the figures are available in Github [78].

Appendix A: Penalty Term and Matrix Product Operator

Since the z component of the total spin corresponds to the total fermion number in the Thirring model, and we are only interested in the zero-charge sector. To enforce this, we introduce a penalty term in the Hamiltonian,

$$\bar{H}^{\text{penalty}} = H + \lambda \left(\sum_{n=0}^{N-1} S_n^z \right)^2. \quad (\text{A1})$$

Here λ should be sufficiently large (100 in this work) to ensure that the ground state obtained via a variational search is in the sector of vanishing total S^z [79], that is, $\langle S_{tot}^z \rangle = \langle \sum_n S_n^z \rangle = 0$. This enables us to interpret our results in terms of the dual SG theory and the XY model. However, the penalty term will not be turned on during the real-time evolution simulations since $\langle S_{tot}^z \rangle$ is a conserved quantity. In our simulations, this quantity is well preserved, i.e., $\langle S_{tot}^z(t) \rangle = 0$.

In TN algorithms, it is useful to express the Hamiltonian as the MPO. The Hamiltonian of Thirring model in Eq. (A1) can be expressed as an MPO:

$$W^{[n]} = \begin{pmatrix} \mathbb{I} & -\frac{1}{2}S^+ & -\frac{1}{2}S^- & 2\lambda S^z & \Delta S^z & \beta_n S^z + \alpha \mathbb{I} \\ 0 & 0 & 0 & 0 & 0 & S^- \\ 0 & 0 & 0 & 0 & 0 & S^+ \\ 0 & 0 & 0 & \mathbb{I} & 0 & S^z \\ 0 & 0 & 0 & 0 & 0 & S^z \\ 0 & 0 & 0 & 0 & 0 & \mathbb{I} \end{pmatrix}. \quad (\text{A2})$$

where $\beta_n = \Delta + (-1)^n \tilde{m}_0 a$, $\alpha = \frac{1}{4}(\lambda + \Delta)$. The β_n contains the staggered term. To simplify the simulation, we also combine two-site MPOs into one site, as we did with the uMPS, represented as $W_1 W_2 \rightarrow W$.

Appendix B: Brief Introduction of VUMPS and TDVP

To prepare the ground state in uMPS form, we use the VUMPS algorithm [58]. In VUMPS, we need to construct the effective Hamiltonian through the MPO and the boundary tensors L, R , which satisfy the fixed-point equations (see Fig. 8).

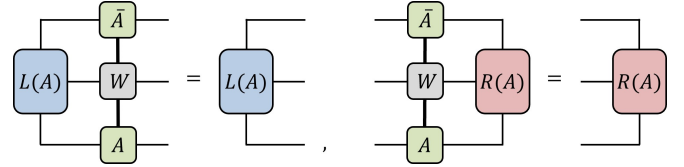
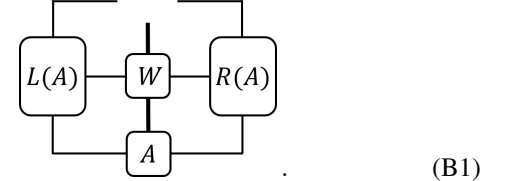


FIG. 8. The fixed-point equations of the boundary tensors L and R .

The tensor diagram of the effective Hamiltonian operating on the unit cell can be expressed as:



The boundary tensors L and R are functions of A . We could use the Lanczos algorithm to obtain the optimal A and then update L and R until it reaches the ground state. In our simulation, we turned on the penalty term λ in Eq. (A2) to guarantee that the ground state we obtained is in the sector of vanishing total $\langle S_z \rangle$.

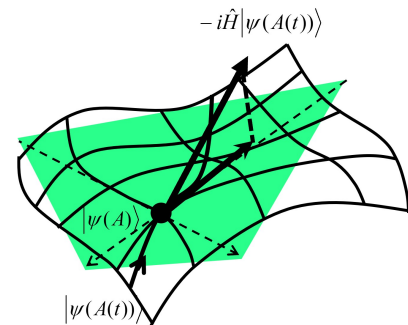


FIG. 9. An illustration of the TDVP. The curve is the manifold of the uMPS and the colored plane is the tangent space of the current state.

For real-time evolution, we choose the TDVP algorithm, which preserves conserved quantities well [73]. TDVP corresponds to a projection of the evolution state of the Schrödinger equation onto the tangent space of the uMPS manifold \mathcal{M} at the current state (see Fig. 9). We can solve the time derivative of the uMPS $|\Psi(A)\rangle$ through the TDVP equation:

$$\frac{\partial}{\partial t} |\Psi(A)\rangle = -i\hat{P}_{T_{|\Psi(A)\rangle}, \mathcal{M}} \hat{H} |\Psi(A)\rangle. \quad (\text{B2})$$

The left-hand side of Eq. (B2) gives the time derivative of the tensor A , while the right-hand side gives the projection result: $-iB$, where B is also a tensor that has the same shape as tensor A . Thus, we will get $\dot{A} = -iB$, which can be solved

using the Runge-Kutta (RK4) method. Note that for real-time evolution, we turn off the penalty term λ in Eq. (A2) (setting $\lambda = 0$).

-
- [1] A. Mitra, Quantum quench dynamics, *Annu. Rev. Condens. Matter Phys.* **9**, 245 (2018).
- [2] M. Heyl, A. Polkovnikov, and S. Kehrein, Dynamical quantum phase transitions in the transverse-field ising model, *Phys. Rev. Lett.* **110**, 135704 (2013).
- [3] M. Heyl, Dynamical quantum phase transitions: a review, *Reports on Progress in Physics* **81**, 054001 (2018).
- [4] G. Torlai, L. Tagliacozzo, and G. D. Chiara, Dynamics of the entanglement spectrum in spin chains, *Journal of Statistical Mechanics: Theory and Experiment* **2014**, P06001 (2014).
- [5] P. Uhrich, N. Defenu, R. Jafari, and J. C. Halimeh, Out-of-equilibrium phase diagram of long-range superconductors, *Phys. Rev. B* **101**, 245148 (2020).
- [6] F. Verstraete, V. Murg, and J. I. Cirac, Matrix product states, projected entangled pair states, and variational renormalization group methods for quantum spin systems, *Adv. Phys.* **57**, 143 (2008).
- [7] U. Schollwöck, The density-matrix renormalization group in the age of matrix product states, *Ann. Phys.* **326**, 96 (2011).
- [8] R. Orús, A practical introduction to tensor networks: Matrix product states and projected entangled pair states, *Annals Phys.* **349**, 117 (2014).
- [9] P. Silvi, F. Tschirsich, M. Gerster, J. Jünemann, D. Jaschke, M. Rizzi, and S. Montangero, The Tensor Networks Anthology: Simulation techniques for many-body quantum lattice systems, *SciPost Phys. Lect. Notes*, 8 (2019).
- [10] K. Okunishi, T. Nishino, and H. Ueda, Developments in the Tensor Network — from Statistical Mechanics to Quantum Entanglement, *J. Phys. Soc. Jpn* **91**, 062001 (2022).
- [11] M. C. Bañuls, Tensor Network Algorithms: A Route Map, *Annu. Rev. Condens. Matter Phys.* **14**, 10.1146/annurev-conmatphys-040721-022705 (2023).
- [12] M. Fannes, B. Nachtergaelie, and R. F. Werner, Finitely correlated states on quantum spin chains, *Commun. Math. Phys.* **144**, 443 (1992).
- [13] S. Östlund and S. Rommer, Thermodynamic limit of density matrix renormalization, *Phys. Rev. Lett.* **75**, 3537 (1995).
- [14] G. Vidal, Efficient classical simulation of slightly entangled quantum computations, *Phys. Rev. Lett.* **91**, 147902 (2003).
- [15] F. Verstraete, D. Porras, and J. I. Cirac, Density matrix renormalization group and periodic boundary conditions: A quantum information perspective, *Phys. Rev. Lett.* **93**, 227205 (2004).
- [16] D. Perez-Garcia, F. Verstraete, M. M. Wolf, and J. I. Cirac, Matrix product state representations, *Quantum Inf. Comput.* **7**, 401 (2007).
- [17] F. Andraschko and J. Sirker, Dynamical quantum phase transitions and the loschmidt echo: A transfer matrix approach, *Phys. Rev. B* **89**, 125120 (2014).
- [18] P. Calabrese and J. L. Cardy, Entanglement entropy and quantum field theory, *J. Stat. Mech.* **0406**, P06002 (2004).
- [19] T. J. Osborne, Efficient approximation of the dynamics of one-dimensional quantum spin systems, *Phys. Rev. Lett.* **97**, 157202 (2006).
- [20] N. Schuch, M. M. Wolf, K. G. H. Vollbrecht, and J. I. Cirac, On entropy growth and the hardness of simulating time evolution, *New J. Phys.* **10**, 033032 (2008).
- [21] J. Haegeman, C. Lubich, I. Oseledets, B. Vandereycken, and F. Verstraete, Unifying time evolution and optimization with matrix product states, *Phys. Rev. B* **94**, 165116 (2016).
- [22] L. Vanderstraeten, J. Haegeman, F. Verstraete, and D. Poilblanc, Quasiparticle interactions in frustrated Heisenberg chains, *Phys. Rev. B* **93**, 235108 (2016).
- [23] S. Paekel, T. Köhler, A. Swoboda, S. R. Manmana, U. Schollwöck, and C. Hubig, Time-evolution methods for matrix-product states, *Annals Phys.* **411**, 167998 (2019).
- [24] C. Karrasch and D. Schuricht, Dynamical quantum phase transitions in the quantum potts chain, *Phys. Rev. B* **95**, 075143 (2017).
- [25] V. Zauner-Stauber and J. C. Halimeh, Probing the anomalous dynamical phase in long-range quantum spin chains through fisher-zero lines, *Phys. Rev. E* **96**, 062118 (2017).
- [26] S. De Nicola, A. A. Michailidis, and M. Serbyn, Entanglement view of dynamical quantum phase transitions, *Phys. Rev. Lett.* **126**, 040602 (2021).
- [27] J. C. Halimeh, D. Trapin, M. Van Damme, and M. Heyl, Local measures of dynamical quantum phase transitions, *Phys. Rev. B* **104**, 075130 (2021).
- [28] J. C. Halimeh, F. Kolley, and I. P. McCulloch, Chebyshev matrix product state approach for time evolution, *Phys. Rev. B* **92**, 115130 (2015).
- [29] M. Van Damme, J.-Y. Desaules, Z. Papić, and J. C. Halimeh, Anatomy of dynamical quantum phase transitions, *Phys. Rev. Res.* **5**, 033090 (2023).
- [30] J. J. Osborne, J. Knaute, I. P. McCulloch, and J. C. Halimeh, Meson mass sets onset time of anomalous dynamical quantum phase transitions (2024), arXiv:2407.03394 [cond-mat.quant-gas].
- [31] P. Jurcevic, H. Shen, P. Hauke, C. Maier, T. Brydges, C. Hempel, B. P. Lanyon, M. Heyl, R. Blatt, and C. F. Roos, Direct observation of dynamical quantum phase transitions in an interacting many-body system, *Phys. Rev. Lett.* **119**, 080501 (2017).
- [32] X.-Y. Guo, C. Yang, Y. Zeng, Y. Peng, H.-K. Li, H. Deng, Y.-R. Jin, S. Chen, D. Zheng, and H. Fan, Observation of a dynamical quantum phase transition by a superconducting qubit simulation, *Phys. Rev. Appl.* **11**, 044080 (2019).
- [33] S. Vajna and B. Dóra, Disentangling dynamical phase transitions from equilibrium phase transitions, *Phys. Rev. B* **89**, 161105 (2014).
- [34] J. C. Halimeh and V. Zauner-Stauber, Dynamical phase diagram of quantum spin chains with long-range interactions, *Phys. Rev. B* **96**, 134427 (2017).
- [35] I. Homrighausen, N. O. Abeling, V. Zauner-Stauber, and J. C. Halimeh, Anomalous dynamical phase in quantum spin chains with long-range interactions, *Phys. Rev. B* **96**, 104436 (2017).
- [36] A. L. Corps and A. Relaño, Dynamical and excited-state quan-

- tum phase transitions in collective systems, Phys. Rev. B **106**, 024311 (2022).
- [37] D. Pérez-García, L. Santilli, and M. Tierz, Dynamical quantum phase transitions from random matrix theory, Quantum **8**, 1271 (2024).
- [38] M. C. Bañuls and K. Cichy, Review on novel methods for lattice gauge theories, Reports on Progress in Physics **83**, 024401 (2020).
- [39] M. C. Bañuls, R. Blatt, J. Catani, A. Celi, J. I. Cirac, M. Dalmonte, L. Fallani, K. Jansen, M. Lewenstein, S. Montangero, C. A. Muschik, B. Reznik, E. Rico, L. Tagliacozzo, K. Van Acoleyen, F. Verstraete, U.-J. Wiese, M. Wingate, J. Zakszewski, and P. Zoller, Simulating lattice gauge theories within quantum technologies, Eur. Phys. J. D **74**, 165 (2020).
- [40] S. D. Bass and E. Zohar, Quantum technologies in particle physics, Phil. Trans. R. Soc. A **380**, 20210072 (2022).
- [41] M. C. Bañuls, K. Cichy, Y.-J. Kao, C. J. David Lin, Y.-P. Lin, and David T. L. Tan, Phase structure of the (1+1)-dimensional massive Thirring model from matrix product states, Phys. Rev. D **100**, 094504 (2019).
- [42] M. Hauru, G. Evenbly, W. W. Ho, D. Gaiotto, and G. Vidal, Topological conformal defects with tensor networks, Phys. Rev. B **94**, 115125 (2016).
- [43] Q. Hu and G. Vidal, Spacetime symmetries and conformal data in the continuous multiscale entanglement renormalization ansatz, Phys. Rev. Lett. **119**, 010603 (2017).
- [44] R. Vanhove, M. Bal, D. J. Williamson, N. Bultinck, J. Haegeman, and F. Verstraete, Mapping topological to conformal field theories through strange correlators, Phys. Rev. Lett. **121**, 177203 (2018).
- [45] B. Buyens, J. Haegeman, K. Van Acoleyen, H. Verschelde, and F. Verstraete, Matrix product states for gauge field theories, Phys. Rev. Lett. **113**, 091601 (2014).
- [46] S. Kühn, E. Zohar, J. I. Cirac, and M. C. Bañuls, Non-Abelian string breaking phenomena with matrix product states, Journal of High Energy Physics **2015**, 130 (2015).
- [47] B. Buyens, J. Haegeman, H. Verschelde, F. Verstraete, and K. Van Acoleyen, Confinement and string breaking for QED₂ in the Hamiltonian picture, Phys. Rev. X **6**, 041040 (2016).
- [48] T. Pichler, M. Dalmonte, E. Rico, P. Zoller, and S. Montangero, Real-time dynamics in U(1) lattice gauge theories with tensor networks, Phys. Rev. X **6**, 011023 (2016).
- [49] P. Schmoll, J. Naumann, A. Nietner, J. Eisert, and S. Sotiriadis, Hamiltonian truncation tensor networks for quantum field theories (2023), arXiv:2312.12506 [quant-ph].
- [50] M. C. Bañuls, K. Cichy, J. I. Cirac, K. Jansen, and H. Saito, Matrix product states for lattice field theories, PoS(LATTICE 2013), 332 (2014).
- [51] S. Peotta, F. Brange, A. Deger, T. Ojanen, and C. Flindt, Determination of dynamical quantum phase transitions in strongly correlated many-body systems using loschmidt cumulants, Phys. Rev. X **11**, 041018 (2021).
- [52] I. McCulloch, Detecting and characterising dynamical quantum phase transitions through higher moments, in *APS March Meeting Abstracts*, Vol. 2023 (APS, New York, 2023) p. B33.001.
- [53] A. K. Das and V. S. Mathur, Path Integral Solubility of Two-Dimensional Models, Phys. Rev. **D33**, 489 (1986).
- [54] J. S. Schwinger, Gauge Invariance and Mass. 2., Phys. Rev. **128**, 2425 (1962).
- [55] C. Hagen, New solutions of the Thirring model, Il Nuovo Cimento **B51**, 169 (1967).
- [56] A. Luther, Eigenvalue spectrum of interacting massive fermions in one-dimension, Phys. Rev. **B14**, 2153 (1976).
- [57] H. N. Phien, G. Vidal, and I. P. McCulloch, Infinite boundary conditions for matrix product state calculations, Phys. Rev. B **86**, 245107 (2012).
- [58] V. Zauner-Stauber, L. Vanderstraeten, M. T. Fishman, F. Verstraete, and J. Haegeman, Variational optimization algorithms for uniform matrix product states, Phys. Rev. B **97**, 045145 (2018).
- [59] D. J. Amit, Y. Y. Goldschmidt, and S. Grinstein, Renormalisation group analysis of the phase transition in the 2d Coulomb gas, sine-Gordon theory and XY-model, Journal of Physics A: Mathematical and General **13**, 585 (1980).
- [60] D. B. Kaplan, J.-W. Lee, D. T. Son, and M. A. Stephanov, Conformality lost, Phys. Rev. D **80**, 125005 (2009).
- [61] J. Zinn-Justin, Quantum field theory at finite temperature: An introduction (2000), arXiv:hep-ph/0005272 [hep-ph].
- [62] J. M. Kosterlitz and D. J. Thouless, Ordering, metastability and phase transitions in two-dimensional systems, J. Phys. **C6**, 1181 (1973).
- [63] J. M. Kosterlitz, The critical properties of the two-dimensional xy model, Journal of Physics C: Solid State Physics **7**, 1046 (1974).
- [64] A. LeClair, G. Mussardo, H. Saleur, and S. Skorik, Boundary energy and boundary states in integrable quantum field theories, Nuclear Physics B **453**, 581 (1995).
- [65] W. van Saarloos and D. A. Kurtze, Location of zeros in the complex temperature plane: Absence of Lee-Yang theorem, Journal of Physics A: Mathematical and General **17**, 1301 (1984).
- [66] C. Karrasch and D. Schuricht, Dynamical phase transitions after quenches in nonintegrable models, Phys. Rev. B **87**, 195104 (2013).
- [67] S. Bandyopadhyay, A. Polkovnikov, and A. Dutta, Observing dynamical quantum phase transitions through quasilocal string operators, Phys. Rev. Lett. **126**, 200602 (2021).
- [68] S. Bandyopadhyay, A. Polkovnikov, and A. Dutta, Late-time critical behavior of local stringlike observables under quantum quenches, Phys. Rev. B **107**, 064105 (2023).
- [69] R. V. Bhat and S. Bera, Distinguishing dynamical quantum criticality through local fidelity distances, Phys. Rev. B **109**, 214313 (2024).
- [70] P. Zhao, J. Sun, S. Jin, Z. Hu, D. Li, X.-J. Liu, J. Schmiedmayer, and X. Chen, Determination of dynamical quantum phase transitions for boson systems using the Loschmidt cumulants method, Phys. Rev. A **109**, 013309 (2024).
- [71] R. Hamazaki, Exceptional dynamical quantum phase transitions in periodically driven systems, Nature Communications **12**, 5108 (2021).
- [72] R. Orús, Advances on tensor network theory: symmetries, fermions, entanglement, and holography, Eur. Phys. J. B **87**, 280 (2014).
- [73] J. Haegeman, J. I. Cirac, T. J. Osborne, I. Pižorn, H. Verschelde, and F. Verstraete, Time-dependent variational principle for quantum lattices, Phys. Rev. Lett. **107**, 070601 (2011).
- [74] A detailed investigation of the equilibration process is beyond the scope of this work.
- [75] M. B. Hastings, Solving gapped Hamiltonians locally, Phys. Rev. B **73**, 085115 (2006).
- [76] A. Molnar, N. Schuch, F. Verstraete, and J. I. Cirac, Approximating Gibbs states of local Hamiltonians efficiently with projected entangled pair states, Phys. Rev. B **91**, 045138 (2015).
- [77] T. Hashizume, I. P. McCulloch, and J. C. Halimeh, Dynamical phase transitions in the two-dimensional transverse-field Ising

- model, Phys. Rev. Res. **4**, 013250 (2022).
- [78] https://github.com/hunghacti/Thirring_data.
- [79] M. C. Bañuls, K. Cichy, J. I. Cirac, and K. Jansen, The mass spectrum of the Schwinger model with matrix product states, J. High Energy Phys. **2013** (11), 158.